

Structure and Morphology of PDI8-CN2 for n-Type Thin-Film Transistors

Fabiola Liscio, Silvia Milita,* Cristiano Albonetti, Pasquale D'Angelo, Antonietta Guagliardi, Norberto Masciocchi, Raffaele Guido Della Valle, Elisabetta Venuti, Aldo Brillante, and Fabio Biscarini

A multiscale investigation of *N,N'*-bis(*n*-octyl)-*x,y*, dicyanoperylene-3,4:9,10-bis(dicarboximide), PDI8-CN2, shows the same molecular arrangement in the bulk and in thin films sublimated on SiO₂/Si wafers. Non-conventional powder diffraction methods and theoretical calculations concur to provide a coherent picture of the crystalline structure. X-ray diffraction (XRD) and atomic force microscopy (AFM) analyses of films of different thickness deposited at different substrate temperatures indicate the existence of two temperature-dependent deposition regimes: a low-temperature (room temperature) regime and a high-temperature (80–120 °C) one, each characterized by different growth mechanisms. These mechanisms eventually result in different morphological and structural features of the films, which appear to be highly correlated with the trend of the electrical parameters that are measured in PDI8-CN2-based field-effect transistors.

1. Introduction

In recent years, polycrystalline organic thin-film transistors (OTFTs) have been the subject of growing scientific and technological interest.^[1–9] Compared with traditional silicon electronics, devices based on organic semiconductors certainly have

appealing characteristics, such as light weight, mechanical flexibility and low-cost production. These advantages make them promising candidates for a wide range of applications such as displays,^[10–12] radio-frequency identification (RF-ID) tags,^[13] and sensors.^[14–17]

To make full use of organic electronic circuitry, it is necessary to combine p-channel and n-channel transistors to produce complementary circuits, which show greater speed, reliability and stability than ambipolar ones.^[18–21] While highly pure, stable and solution-processable p-type materials with a charge mobility of 1–10 cm² V^{−1} s^{−1} are nowadays available in production amounts,^[22–27] n-type organic semiconductors of high air-stability and mobility are still a topic of research.

Indeed, in the past few years, several high-performance n-type semiconductors have been developed, which also exhibit a high stability in ambient conditions, mostly used as films obtained from vapor deposition methods.^[28,29] More recently, solution-processable and printable n-type semiconductors, both small molecules and polymers,^[30–33] have been reported, allowing unprecedented OTFT characteristics. Perylene di-imide derivatives are considered to be among the most important n-type organic materials because of their relatively strong electron affinities and the tailoring of the charge-transport properties upon changing the substituents on the imide N atoms or on the perylene backbone.^[34–42]

In this paper, we focus on *N,N'*-bis(*n*-octyl)-*x,y*, dicyanoperylene-3,4:9,10-bis(dicarboximide), PDI8-CN2, a derivative having two cyano groups directly bound to the aromatic core, which has been proved to be a suitable material for complementary circuits^[43] and shown to yield high-performance devices by sublimation or from solution methods.^[44]

In spite of the potential of PDI8-CN2 and the importance attributed to the control of grain boundary effects in small-molecule device performance and reproducibility, experimentally derived knowledge of the crystal structure and molecular conformation and how these factors affect the multiscale organization and microstructure in the film phase are still missing. The packing motif proposed by Rivnay et al.^[44] relies on the combination of the X-ray scattering of thin films and pseudo-potential calculations, which is not as robust or conclusive as

Dr. F. Liscio, Dr. S. Milita
CNR-IMM, Istituto per la Microelettronica e Microsistemi
Via P. Gobetti 101, I-40129 Bologna, Italy
E-mail: milita@bo.imm.cnr.it

Dr. C. Albonetti, Dr. P. D'Angelo,^[+] Prof. F. Biscarini
CNR-ISMN, Istituto per lo Studio dei Materiali Nanostrutturati
Via P. Gobetti 101, I-40129 Bologna, Italy

Dr. A. Guagliardi^[++]
CNR-IC, Istituto di Cristallografia
Via Amendola 122/O, 70126 Bari, Italy

Prof. N. Masciocchi
Dipartimento di Scienze Chimiche e Ambientali
Università dell'Insubria
Via Valleggio 11, I-22100 Como, Italy

Prof. R. G. Della Valle, Dr. E. Venuti, Prof. A. Brillante
Dipartimento Chimica Fisica Inorganica
Viale Risorgimento 4, I-40136 Bologna, Italy

[+] Present address: Chemistry Department, Imperial College London,
Exhibition Road, South Kensington, London SW7 2AZ, UK

[++] Present address: Dipartimento di Scienze Chimiche e Ambientali,
Università dell'Insubria, Via Valleggio 11, I-22100 Como, Italy



DOI: 10.1002/adfm.201101640

single-crystal and powder diffraction crystallographic structure determination methods. A correlation between the structural and charge transport properties in PDI8-CN2 films has not yet exhaustively been established. Sublimation was chosen as the most controllable fabrication method, although the obtained results could easily be applied to systems obtained from solution. Indeed, the presence of the same crystal phase in films prepared from solution and by sublimation has been reported recently, although vapor-phase deposition affords films that are more highly textured than those from solution processing.^[45] This evidence entitled Rivnay et al. to study evaporated thin films suitable for quantitative analysis, in order to propose their crystal-phase model.^[44]

Since we were not able to grow crystalline samples of suitable size and quality for a complete, single-crystal structural analysis, we opted for a less conventional structural powder diffraction method, from which we successfully retrieved otherwise inaccessible structural information. This approach is possible when the molecular complexity is not too high. Due to the accuracy level inherent in the collapse of the 3D diffraction pattern to a single axis, which is typical of a powder diffraction trace, and due to the limited scattering power of the organic material, we decided to further validate the structural model by means of *ab initio* and molecular-mechanics (MM) calculations. Once the crystal structure of the bulk material was assessed, a fruitful comparison with the structure of the thin film phase was established by ancillary diffraction methods; finally, the dependence of the device performance on the film structure, morphology and growth mechanism was investigated for different thicknesses and substrate temperatures during the deposition.

The paper is organized as follows: the crystal structure of PDI8-CN2 in the bulk material and in the film is described in Section 2; Section 3 deals with the structural and morphological dependence of PDI8-CN2 films on substrate temperature and thickness; Section 4 is dedicated to the discussion of the experimental results with the purpose of elucidating the OTFT performances and the main conclusions are also drawn in this section.

2. The Crystal Structure of PDI8-CN2

2.1. The Crystal Structure of the Bulk

A convincing crystal structure arrangement was extracted by coupling diffraction data from two different experimental setups (a conventional para-focusing Bragg–Brentano θ : θ goniometer and a Debye–Scherrer diffractometer)^[46] in order to limit undesired experimental effects imposed by the acicular shape of the crystals (vide infra). These data were analyzed by the fairly complex approach described in the Supporting Information, with the aid of the theoretical prediction/validation reported below. The parameters of the reduced unit cell of powder PDI8-CN2 (P-PD), shown in Table 1, are somewhat similar, but not

Table 1. Lattice parameters of PDI8-CN2, refined from powders (XRPD) and thin films (GID).^[44] The last row refers to calculated values from MM simulations.

| | <i>a</i> [Å] | <i>b</i> [Å] | <i>c</i> [Å] | α [°] | β [°] | γ [°] | <i>V</i> [Å ³] |
|-----------------------|-----------------|-----------------|-----------------|-----------------|----------------|-----------------|-------------------------------|
| XRPD | 5.019 | 8.841 | 20.195 | 101.51 | 92.33 | 100.15 | 862 |
| GID, Rivnay (reduced) | 5.028 | 8.930 | 19.944 | 99.8 | 90.6 | 100.7 | 867 |
| MM, this work | 5.081 | 8.516 | 21.260 | 97.8 | 99.0 | 96.5 | 892 |

identical, to those previously reported for thin films^[44] after cell reduction (TF-PD). Both the proposed unit cells are triclinic and share two axes (*a*, *b*) and interaxial angle (here γ), whereas they slightly differ in *c*-axis length and, to a minor extent, direction. These results suggest that the TF-PD and P-PD materials likely belong to the same crystal phase. However, the molecular arrangement of the structural model that best fits the observed powder diffraction traces, derived by the non-conventional structure solution and full pattern refinements performed by simultaneously using both the datasets discussed above (Figure SI.1 and Table SI.1, Supporting Information), is markedly different from that originally proposed and is shown, in projection, in the drawing in Figure 1a.

In the crystal structure of P-PD that we have derived, the planar centrosymmetric perylene cores stack cofacially by the short π – π contact of approximately 3.40 Å, a typical intermolecular distance between adjacent aromatic planes of perylene cores.^[47] It is noteworthy that the hexagonal rings generating this infinite stack are shifted on top of each other in the ABCABC sequence, typical of the rhombohedral stacking of graphene sheets^[48] and not of ordinary hexagonal graphite. Figure 1b shows a molecular stack (along the [−651] direction) of the aromatic cores with the

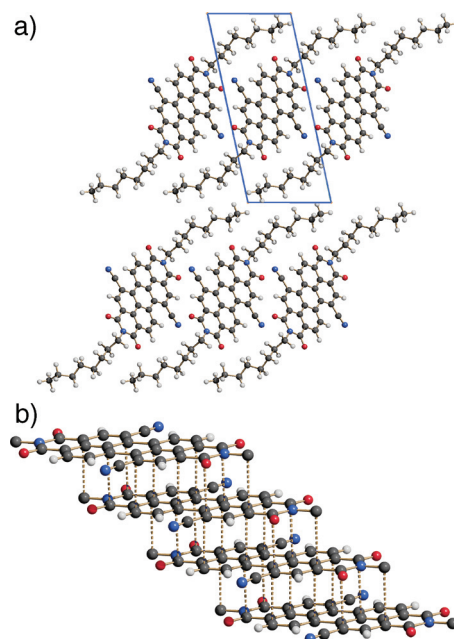


Figure 1. a) Schematic drawing of the crystal structure of PDI8-CN2, viewed down [100]; horizontal axis = *b*. The absence of alkyl-chain interdigitation in the *c* direction, originally proposed by Rivnay et al.^[44] is evident. b) π – π stacking of the flat perylene cores in the ABCA sequence (side chains omitted for clarity). The molecules stack along the [−651] vector.

short van der Waals interactions drawn as dotted lines.^[49–51] The slippage angle (i.e., the angle between the vector normal to the aromatic planes and the vector joining the centers of the two adjacent PDI8-CN2 molecules) is 51° . This value approaches the magic angle value of 54.7° ,^[52] suggesting that the packing of PDI8-CN2 molecules in the film resembles a J-type aggregation. This result is in agreement with the reported UV–vis absorption spectrum of PDI8-CN2 films,^[53] red shifted with respect to that of the molecules in diluted solution.

Interestingly, the prototypical all-*trans* conformation of the long alkyl chains^[44] is absent here. The pertinent refined torsion angles, reported in the Supporting Information, result in an approximate *ttgtt* chain conformation (*t* = *trans*, *g* = *gauche*). In the crystal, a few weak H-bond interactions exist, involving the cyano ($\text{CH}\cdots\text{NC} = 2.43 \text{ \AA}$) and the oxo ($\text{CH}\cdots\text{OC} = 2.43 \text{ \AA}$) residues, falling in the range of weakly attractive (stabilizing) contacts. The slip-stacked motif and the intermolecular contacts between the aromatic planes are similar to those observed in related perylene derivatives, namely PTCDI-C8^[54] and PDI4-CN2.^[35] However, due to the absence of CN groups in the former case and the shorter alkyl chains in the latter, the mentioned intermolecular interactions do not take place and a different alkyl-chain configuration is favored.

Our P-PD refined model does not match the entropically disfavored interdigitation pattern of the long alkyls proposed on the basis of molecular modeling simulations.^[44] Coupled with the possible reduced accuracy inherent to the powder method, this prompted us to investigate the origin of such a discrepancy in depth. Therefore, the experimentally derived crystal structure was validated by means of *ab initio* (gas-phase) and molecular mechanics (in the crystal) energy-minimization calculations, together with a crystal structure search^[55,56] in a reduced subspace. Such a subspace was defined by the assessed information about the crystal (namely, the unit cell parameters and the symmetry). This procedure was aimed at identifying the position of the P-PD model in the energy landscape of the many energetically accessible structures of this compound.

Ab initio calculations performed on isolated PDI8-CN2 molecules showed that the experimentally determined P-PD conformation converges to a local energy minimum, less stable by $1.58 \text{ kcal mol}^{-1}$ than the all-*trans* isomer. In lattice energy calculations, the experimental P-PD structure was found to converge to the deepest minimum of the potential energy surface. The attained minimum was also the most frequently encountered in the structure search, and must therefore correspond to a large attraction basin of the energy surface. Finally, the X-ray diffraction pattern computed for this calculated structure showed a very good agreement with the P-PD data. These results test the quality of the adopted potential model and enable a separate check of the reliability of the experimental molecular packing and geometry. Once the constraints on the lattice parameters were finally removed, a new deep minimum was attained, with lattice parameters shown in Table 1 and in fair agreement with the P-PD ones, but with a slightly inflated volume, by about 3%. It is worth noting that the computed versus the experimental cell volumes of the PDI-*n* analogues (Table SI.2, Supporting Information) show similar inflation, and therefore appear to be inherent in the computational

model. Moreover, the alkyl chains of the compound in the computed structure are still in a bent conformation, much like the experimental one.

2.2. The Crystal Structure of the Thin Films

After determining the P-PD structure, we turned our attention to the PDI8-CN2 films, combining X-ray diffraction (XRD) measurements performed in specular and grazing incidence diffraction (GID) geometries. As an example, we considered a 100 nm-thick film sublimed on a 200 nm-thick SiO_2/Si substrate at $T_{\text{sub}} = 120^\circ\text{C}$, whose typical 2D-GID image is shown in Figure 2a. The perfect symmetry of the spot distribution with respect to the central vertical line implies a fiber-like symmetry of the molecular orientation,^[57] with the long inertial axis almost normal to the substrate surface, (i.e., with the *ab* plane parallel to the substrate surface and *c** normal to it), as confirmed by the specular scans (*vide infra*). Thanks to the knowledge of the domain orientation and of the triclinic lattice symmetry, all of the reflections could be indexed. The presence of the 010 reflection in the 2D-GID image indicates that the projection of the structure on the *a***b** plane did not

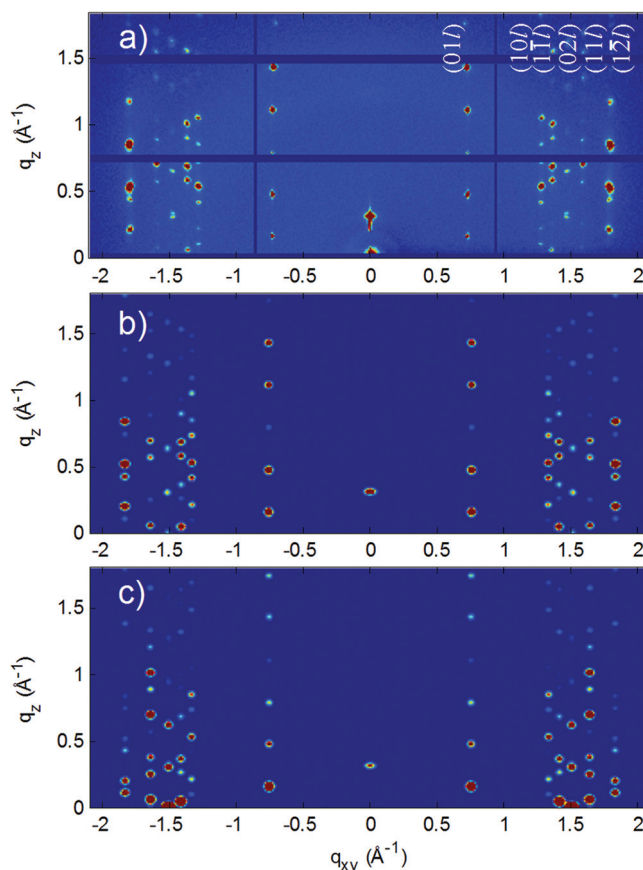


Figure 2. a) Experimental 2D-GID image of PDI8-CN2 film ($t = 100 \text{ nm}$ and $T_{\text{sub}} = 120^\circ\text{C}$) performed with X-ray wavelength $\lambda = 0.8499 \text{ \AA}$ and an incidence angle $\alpha_i = 0.15^\circ$. Simulated 2D-GID image reproduced by using the P-PD structure (b) and a structure with interdigitated alky chains (c).^[44]

have p2gg symmetry, excluding a molecular arrangement in the herringbone configuration,^[58] in agreement with the bulk phase structure. The unit cell parameters extracted from the Bragg positions in the 2D-GID image (q_{xy} and q_z values) and in the specular scan^[59] fairly match those of the bulk phase that are reported in Table 1. The simulated 2D-GID image^[60] for a polycrystalline film with the P-PD crystal structure is shown in Figure 2b. The good agreement between the simulated and the experimental images, in particular, of their spot intensities, allowed us to establish that the molecular packing in the film was the same as the powder bulk phase. Indeed, a small deviation in the atomic positions and in the molecular orientation has a pronounced effect on the intensity distribution and a substantial discrepancy was observed when a crystal structure with interdigitated chains (such as that proposed by Rivnay et al.^[44]) was considered (see Figure 2c).

The invariance of the molecular packing in the films and in the bulk differs from what is observed for other perylene derivatives (i.e., PTCDI-C8^[61,62] and PTCDI-C5^[37,63,64]), where the c lattice parameter of the thin-film structure is found to be significantly larger and the tilt angle of the aromatic core relative to the ab plane is found to be slightly smaller than those of the bulk case. For PTCDI-C5 molecules,^[37] a thin film phase was observed for films deposited at $T_{\text{sub}} < 125$ °C, whereas films grown at a higher temperature possessed the bulk phase structure. In such a case, the thin-film structure was identified as being a metastable growth-limited phase of a thermodynamically stable polymorph. Liquid crystalline phases and polymorphism are indeed well documented in the perylene di-imide family of molecules.^[64] Differently, our results can be interpreted by the presence of the CN groups, which impose geometrically stiff intermolecular interactions, basically unaffected by molecule-substrate interactions. The structural similarity of the film and bulk materials and knowledge of their common crystalline structure allows us to evaluate the tilting of the average polyaromatic molecular planes with respect to the surface of the film (taken as the ab plane), estimated to be 68.1°. It follows that the molecules stack with π - π interactions almost perpendicular to the substrate surface, which is relevant information for interpreting the charge carrier transport mechanism. However, as discussed in the following section, a small variability of the lattice parameters was observed for films prepared under different conditions, but, on the basis of the extracted values, we consider it too small to invoke the presence of an independent thin-film phase; accordingly, we prefer to interpret this effect as a slight distortion of the bulk phase, rather than as the existence of new polymorphic forms.

3. The Dependence of the PDI8-CN2 Film Structure and Morphology on T_{sub} and the Film Thickness t

PDI8-CN2 films of three different thicknesses (10, 40, and 100 nm) were deposited by high-vacuum sublimation (HVS) ($P = 2 \times 10^{-8}$ mbar) at a rate of 12.5 Å min^{-1} on a 200 nm-thick SiO₂ substrate thermally grown on a (001) Si wafer. Three series of films were prepared by keeping the substrate temperature, T_{sub} , at 25 °C (room temperature (RT)), 80 °C and 120 °C during the deposition.

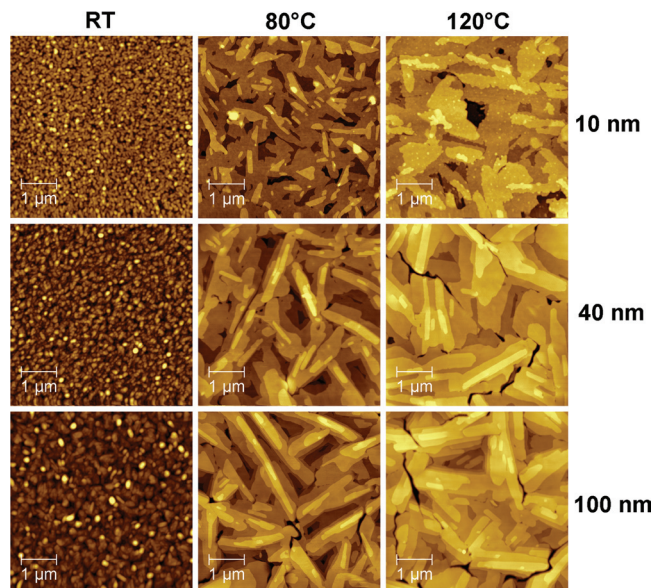


Figure 3. AFM images of PDI8-CN₂ films of different thicknesses (10 nm, 40 nm and 100 nm) deposited at $T_{\text{sub}} = \text{RT}$, 80 °C and 120 °C.

3.1. Morphology Variability of the PDI8-CN2 Films on T_{sub} and t

The morphology of the PDI8-CN2 films was characterized using atomic force microscopy (AFM) in intermittent contact mode configuration. The topographic images, recorded on surface regions with a lateral size of 5 μm (Figure 3) show a clear dependence on both T_{sub} and the film thickness t .

For all of the T_{sub} values, the grain and island sizes increased with t without any significant changes in shape.

The films grown at RT were formed by small grains with sizes ranging from 60 nm ($t = 10$ nm) to 100 nm ($t = 100$ nm), whereas those grown at 80 °C and 120 °C consisted of large terraces, a few micrometers long. The terraces were characterized by molecular steps 17 ± 2 Å high, a value close to the $d_{(001)}$ spacing (≈ 19.7 Å), as determined by the XRD measurements (see above). In the thicker ones ($t = 100$ nm), the terraces were covered by elongated islands, which are commonly observed in other perylene derivatives, and are due to an anisotropic 2D growth.^[61]

In addition, we noticed that films grown at 120 °C revealed crack formation. The thermal expansion coefficient for the organic film is likely to be more than an order of magnitude larger than that of the SiO₂ substrate. Therefore, upon cooling, the film was put under tension and underwent cracking. As expected, films with severe cracking yielded OTFTs with diminished carrier mobility and significant threshold instability.

For each sample, the root-mean-square roughness, σ_{surf} , was determined as the standard deviation of the film height distribution averaged over three topographic images with a lateral size of 30 μm (Table SI.3, Supporting Information). Figure 4a shows a log-log plot of σ_{surf} as a function of t for the films deposited at the three values of T_{sub} . Regardless of T_{sub} , σ_{surf} increased with t , and the surface roughening was faster at RT. Indeed, in the films 10 and 40 nm thick, σ_{surf} attained approximately ≈ 14 Å and ≈ 20 Å, respectively, for all of the values of T_{sub} , while at RT,

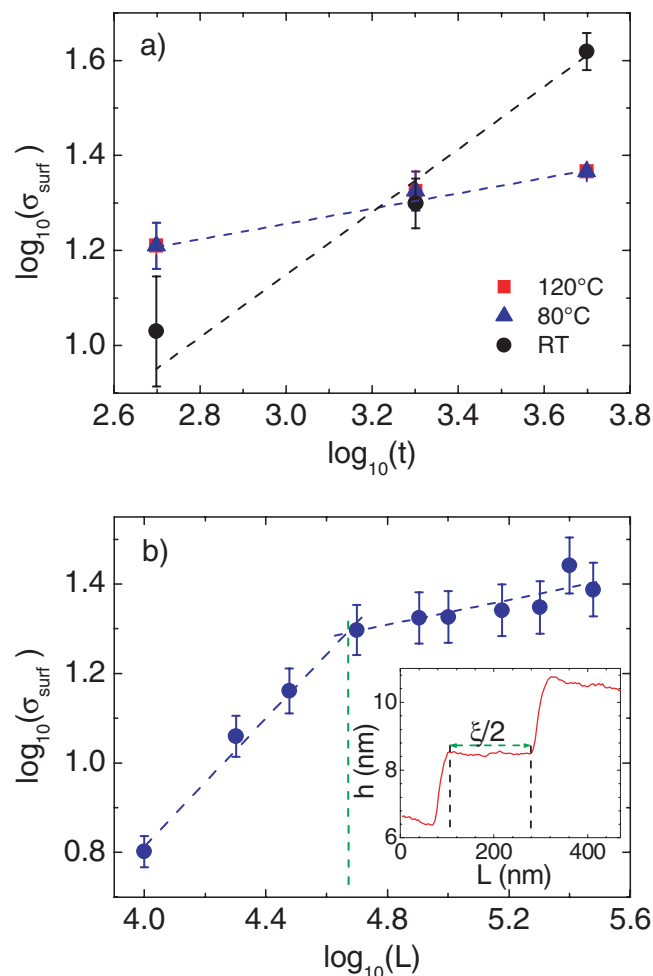


Figure 4. a) Log–log plot of σ_{surf} versus film thickness. The blue dots indicate data for $T_{\text{sub}} = \text{RT}$, the red squares for $T_{\text{sub}} = 80$ °C and the green diamonds for $T_{\text{sub}} = 120$ °C. The fitting lines are reported as dashed lines of the corresponding colours. b) Log–log plot of σ_{surf} versus L for PDI8-CN2 films, 100 nm thick, grown at $T_{\text{sub}} = 80$ °C. Inset: PDI8-CN2 terraces with step $\xi/2$ wide and ≈ 17 Å high.

the σ_{surf} of the 100 nm film was almost twice (≈ 42 Å) the value measured at 80 °C (25 Å) and 120 °C (23 Å). As predicted by dynamic scaling theory (DST),^[65] σ_{surf} evolves with t according to a power law $\sigma_{\text{surf}} \propto t^\beta$, where β is the growth exponent. β spans the interval [0, 1] and generally varies from 0 to 0.5 for compact and flat surfaces, while it exceeds 0.5 for mounded surfaces. In our case, for films grown at RT, β was 0.69 ± 0.09 , suggesting an anomalous growth, commonly termed rapid roughening and previously reported for both organic^[66–68] and inorganic thin films.^[69] This roughening is induced by morphological instabilities of the film, usually associated with a reduced interlayer transport^[70] and is typical of mounded surfaces formed by small grains and highly crystalline clusters (white points in the AFM images of Figure 3). On the other hand, the β values for films grown at higher values of T_{sub} (80 °C and 120 °C) were lower and similar (0.21 ± 0.02 and 0.15 ± 0.04 , respectively), indicating the permanence of their very compact and flat surfaces. In this case, the growth mechanism was close to layer-by-layer, because

the higher T promotes surface smoothening by enhancing the surface diffusion of the organic molecules.^[71–73]

Furthermore, DST predicts that σ_{surf} increases with the lateral size L of the image for a fixed t and follows a power law, $\sigma_{\text{surf}}(L, t) = \mu L^\alpha$, where α is the roughness exponent. α was extracted by plotting σ_{surf} versus L in log–log scale, where σ_{surf} was measured from topographic images with different L , ranging from 1 to 30 μm . Figure 4b shows the plot for the 100 nm-thick PDI8-CN2 film, grown at 80 °C. Similar results were observed for the other cases. Regardless of T_{sub} , for the thickest films (i.e., 100 nm), multiscale surface evolution was highlighted by the appearance of two different slopes in the curve (α' and α) with a characteristic length scale $\xi \approx 5$ μm (dashed line in Figure 4b). This effect suggests two different regimes of surface fluctuations with respect to the lateral size L , which are identified by global (α) and local (α') roughness exponents in the ranges $1 \mu\text{m} \leq L \leq 5 \mu\text{m}$ and $5 \mu\text{m} \leq L \leq 30 \mu\text{m}$, respectively. Note that the global and local surface fluctuation images represent the height undulation of the grains and molecular-step accumulations. The global roughness exponent $\alpha \approx 0.12 \pm 0.04$, averaged for all of the samples, suggests that all the films were smooth over large areas. The local roughness exponent was observed only for the 100 nm films for growth at RT and 80 °C, and for all thicknesses at 120 °C. For the film grown at RT, the α' value of 0.30 ± 0.09 is in agreement with the observed anomalous scaling behavior,^[73] while at the higher values of T_{sub} (80 °C and 120 °C), the value of 0.59 ± 0.09 is consistent with a lamella growth mechanism.^[71,74,75] These results are supported by a measure of the correlation length, ξ , extracted from AFM images^[76] (Supporting Information). As suggested by Biscarini et al.,^[75] ξ increases by increasing both t and T_{sub} . At RT, ξ ranges from 70 to 170 nm with increasing t , in agreement with the average grain sizes evaluated by statistics on the grain diameter distribution (the diameters run from 60 to 100 nm with increasing t).^[77] At 80 °C and 120 °C, ξ increases from 300 to 650 nm with increasing t as a consequence of the highly diffusive motion induced by T_{sub} .^[75,77–79] At the highest T_{sub} , the width of the flat terraces is given by $\xi/2$ (corresponding to the averaged step width, α , see inset in Figure 4b) and σ_{surf} is comparable to that of SiO_2 (5 Å). The values of the exponents β and α of all of the films investigated are reported in Table S1.4, Supporting Information.

3.2. Evolution of the Structure of the PDI8-CN2 Films with T_{sub} and t

The crystalline structures of the three series of PDI8-CN2 films ($T_{\text{sub}} = \text{RT}$, 80 °C and 120 °C) were investigated using XRD measurements performed in specular and GID geometries.

The 2D-GID images of the films prepared at RT and 120 °C, collected with $\lambda = 0.8499$ Å and $\alpha_i = 0.15^\circ$, are reported in Figure 5. Since $\alpha_i > \alpha_{\text{c, film}} = 0.12^\circ$, the beam penetration depth exceeded the film thickness, and the resulting data provide structural information on the whole organic film. All of the films were polycrystalline with the <001> fiber-like texturing described before (see Section 2. 1) (i.e., the crystallites were organized with the ab plane parallel to the surface and with a random in-plane orientation). In spite of the markedly different

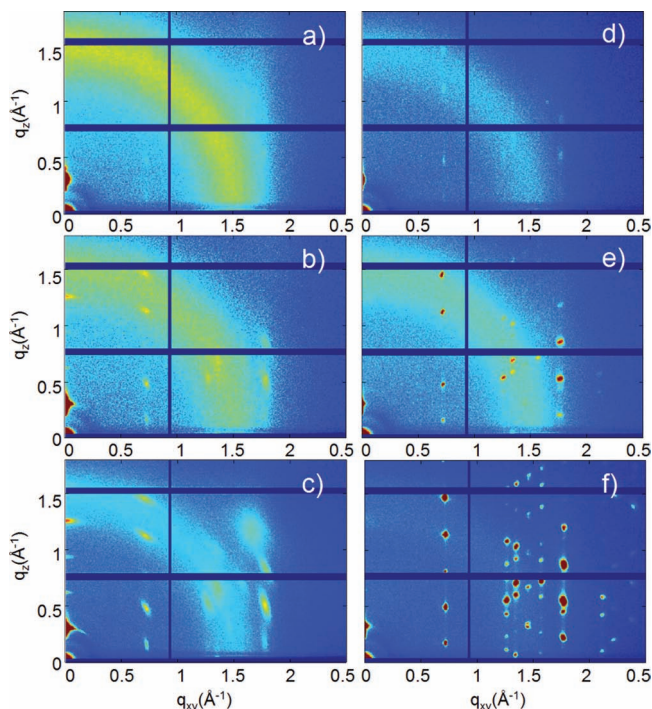


Figure 5. a–f) 2D-GID images of PDI8-CN2 films with nominal thickness of 10, 40 and 100 nm, sublimated on SiO₂ at RT (a–c) and 120 °C (d–f). The measurements were carried out with $\lambda = 0.8499$ Å, an incidence angle $\alpha_i = 0.15^\circ$ and using a 2D Pilatus detector.

film morphologies of the films deposited at the two T_{sub} (see Figure 3), the invariance of the q_{xyz} positions of the reflections, in the limit of the technique's resolution, indicates that the same crystalline structure was present and persisted for all of the thicknesses (10, 40 and 100 nm). The fact that the crystalline structure remained almost unchanged (with the caveats discussed later), from the substrate up to the film surface, was confirmed by the lack of any significant difference in the reflection positions in the 2D-GID images recorded at $\alpha_i = 0.03^\circ$, $\alpha_i \ll \alpha_{\text{c, film}}$ (not shown here), where the signals originated from a surface layer a few Ångströms thick. However, a pronounced difference between the two values of T_{sub} could be observed regarding both the shape and intensity of the diffraction peaks. For the RT films, the arched shape of the Bragg spots, together with the presence of reflections in the specular region ($q_{\text{xy}} = 0$), indicate a large distribution of orientations of the *ab* plane (FigureSI.3, Supporting Information), otherwise negligible at 120 °C. The lower peak intensity values observed for the RT films are then likely attributed to a much wider peak width in the azimuthal (and not radial) direction, although structural effects, such as modified static Debye–Waller factors, which would point to disorder or significantly enhanced molecular mobility, are not precluded.

High-resolution XRD measurements provided interesting additional information. For all of the films, the specular scans ($\omega/2\theta$

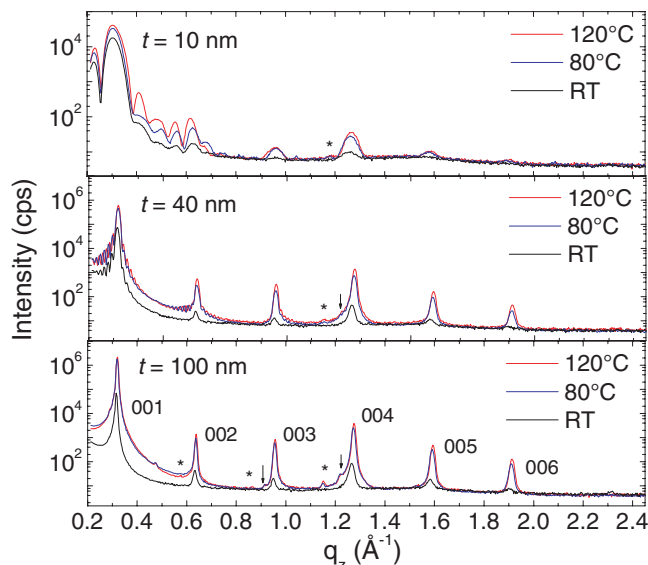


Figure 6. Specular XRD scans of PDI8-CN2 films of different nominal thicknesses (10, 40 and 100 nm) sublimated on SiO₂ at RT (black line), 80 °C (blue line) and 120 °C (red line). The arrows and the stars indicate the reflections generated by the undesired W L α and Cu K β wavelengths.

scans reported in q_z scale, where $q_z = 4\pi\sin\theta/\lambda$, in Figure 6) and the (004) rocking curves (RCs) (ω scans recorded around the 004 peak shown in Figure 7) allowed the extraction of several microstructural parameters, which are reported in Table 2.

A close inspection of the specular scans indicates that the absolute intensities nearly scale with t^2 , as expected for a mass effect, and that the RT films show systematically lower values, probably because of the mentioned wide spread in the reciprocal space. This effect is clearly observed in the plots collected in Figure 7, which show that the peak widths (full width at half-maximum (FWHM) of the (004) RCs), a measure of the angular spread of the orientations of the crystallites, approach or exceed the 2.0° value for the RT films, and shrink to nearly 0.03° for the 80 °C and 120 °C films. In other words, T_{sub} drives the film texturing, manifested by the change of the widths of the (004) RCs, which is a direct measure of the spreading of orientations of the (001) lattice plane about the substrate normal. For the two higher values of T_{sub} , a broad component due to diffusive scattering (DS) is also observed and can be ascribed to structural

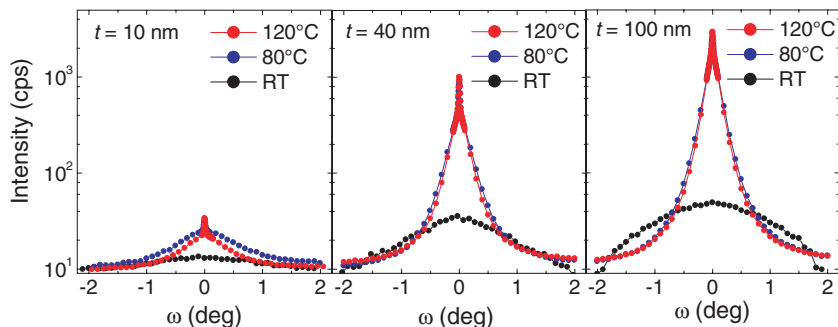


Figure 7. (004) RCs of the PDI8-CN2 films of nominal thicknesses 10, 40 and 100, sublimated at RT (black dots), 80 °C (blue dots) and 120 °C (red dots).

Table 2. Structural parameters determined by specular scans and (004) RC measurements of PDI8-CN2 films: thickness, t ; $d_{(001)}$; domain size along the surface normal, D_{perp} ; and FWHM of (004) RCs.

| T_{sub} [°C] | t [nm] | $d_{(001)}$ [Å] | D_{perp} [nm] | FWHM ₍₀₀₄₎ [°] |
|--------------------------|--------------|--------------------|---------------------------|------------------------------|
| RT | 9.50 ± 0.03 | 19.99 ± 0.03 | 11 ± 1 | 1.9 ± 0.1 |
| RT | 42.5 ± 0.2 | 19.90 ± 0.03 | 33 ± 1 | 1.70 ± 0.02 |
| RT | 100.9 ± 0.2 | 19.85 ± 0.03 | 35 ± 1 | 2.59 ± 0.07 |
| 80 | 10.23 ± 0.08 | 19.92 ± 0.03 | 12 ± 1 | 0.033 ± 0.001 |
| 80 | 38.9 ± 0.3 | 19.77 ± 0.03 | 40 ± 1 | 0.0321 ± 0.0003 |
| 80 | 88.4 ± 0.3 | 19.75 ± 0.03 | 50 ± 1 | 0.0356 ± 0.0006 |
| 120 | 11.19 ± 0.02 | 19.85 ± 0.03 | 13 ± 1 | 0.034 ± 0.001 |
| 120 | 44.58 ± 0.01 | 19.73 ± 0.03 | 40 ± 1 | 0.0339 ± 0.0005 |
| 120 | 103.7 ± 0.1 | 19.71 ± 0.03 | 50 ± 1 | 0.0352 ± 0.0008 |

defects present in the crystalline domains.^[80,81] In pentacene films, the width of the DS contribution was related to the density of dislocations^[58] created during the film growth. Interestingly, in our case, the DS width was found to decrease with increasing film thickness, attaining $\approx 1.0^\circ$ ($t = 10$ nm), $\approx 0.34^\circ$ ($t = 40$ nm) and 0.25° ($t = 100$ nm), at the two higher values of T_{sub} . This suggests that at higher values of T_{sub} , structural defects are generated mainly in the first stage of the growth (thinner films) and partially anneal during deposition (thicker films).^[79,82]

The presence of the Laue oscillations around the (001) peak in the specular scans was observed for all of the samples except the thickest, where the oscillation period was too short to be experimentally resolved. These oscillations, more pronounced for the higher values of T_{sub} (80 °C and 120 °C), are evidence of the coherent nature of the film (along the depth profile), built upon a regular stacking of ordered monolayers (ML).

The PDI8-CN2 $d_{(001)}$ interlayer spacing was determined by accurate analysis of the (004) Bragg peak, which was intense and not affected by the overlapping of the Laue fringes. The $d_{(001)}$ values determined for all of the films (Table 2) showed a slight dependence on both t and T_{sub} . As pictorially shown in Figure 8, $d_{(001)}$ decreased with increasing t ; for constant t , it decreased with T_{sub} , approaching the value measured for P-PD ($d_{(001)} = 19.73$ Å). It is noteworthy that such small changes in

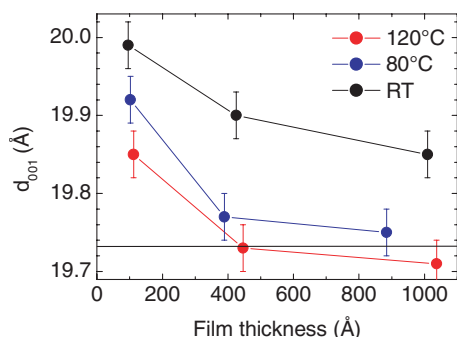


Figure 8. Plot of the $d_{(001)}$ spacing (Å) versus thickness (Å) for the different films and temperature of the substrate during deposition. The thin solid lines are a guide to the eye. The horizontal line at 19.73 Å refers to the value determined for bulk powders from XRPD.

the d spacing could not be detected when using the GID geometry with the 2D-detector setup, and, consistently, did not make the purported constancy of the lattice metrics, and hence the crystal structure, vanish.

The observed structural features can be explained by assuming a progressive molecular rearrangement along the film thickness. This is a common phenomenon for organic molecules where a thin-film phase is often identified by a $d_{(001)}$ value larger than that of the bulk-phase^[83–87] (i.e., molecules align more perpendicularly to the substrate due to the stronger molecules-substrate interaction), resulting into a positively strained c value.

High-resolution diffraction measurements allowed the domain sizes, $D_{\text{perp(par)}}$, to be determined along the directions perpendicular and parallel to the substrate surface, via the relation $D_{\text{perp(par)}} = 2\pi/\Delta q_{z(xy)}$.^[57] The D_{perp} values, estimated from analysis of the (004) peaks, are reported in Table 2. For all of the values of T_{sub} , the D_{perp} value of the 10 nm film matched the film thickness (≈ 5 ML), whereas that of the thickest (100 nm) did not attain the thickness value and was larger (50 nm (i.e., ≈ 25 ML)) at the higher T_{sub} values (80 °C and 120 °C) than at RT (35 nm (i.e., 16 ML)). This indicates that the molecules were stacked perfectly in the first 16 ML (RT) and 25 ML (80 °C and 120 °C), on average, before the occurrence of defects inducing the loss of X-ray diffraction coherence.

On the other hand, for the thickest films, the mean lateral size, D_{par} , of the crystalline domains was estimated by analysis of the ($hk0$) reflections, recorded through the high-resolution GID in-plane measurements (shown in Figure 9). For the RT films, $D_{\text{par}} = 19$ nm (averaged along three different crystallographic directions, 010, 100 and 1–10), whereas for the 120 °C films, D_{par} was approximately 40% larger. Although the D_{par} values were found to be larger than those observed for the RT film, they were considerably smaller than the characteristic grain length of few micrometers, observed by AFM (Figure 3). This means that the grains were formed by several crystallographic domains, a result consistent with previous experimental evidence on sexithienyl films.^[88]

4. Discussion and Conclusions

The structural and morphological results enable the interpretation of the behavior of PDI8-CN2-based field-effect

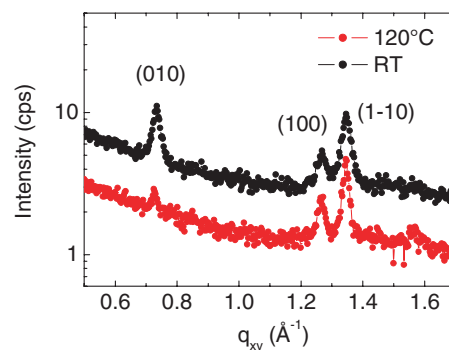


Figure 9. High-resolution GID in-plane scans of 100 nm-thick PDI8-CN2 films deposited at RT (black) and 120 °C (red). The scans are vertically shifted for clarity.

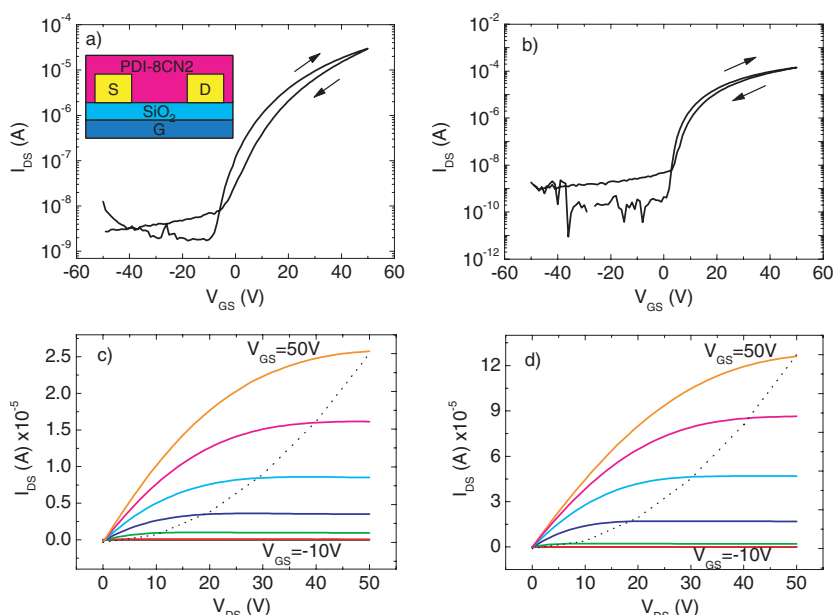


Figure 10. a,b) Performances of OTFTs based on 40 nm PDI8-CN2 film recorded in air: transfer characteristics for films grown at RT (a) and 120 °C (b) in the saturation regime ($V_{DS} = 50$ V). The arrows indicate the gate-voltage-sweep direction. The layout of the used bottom-contact bottom-gate OTFT is shown in the inset to (a). c,d) Output characteristics for films grown at RT (c) and at 120 °C (d).

transistors (FETs). The electrical characteristics of OTFTs in bottom-contact geometry (a sketch of which is reported in the inset of Figure 10a), were measured both in air and under vacuum (10^{-4} mbar) by averaging the values over four devices for two representative values of T_{sub} (i.e., RT and 120 °C).

Figure 10a,b present the typical transfer curves recorded in air for OTFTs based on 40 nm-thick PDI8-CN2 films deposited at RT and 120 °C, respectively. An enhancement of the I_{DS} values and a reduction of the hysteresis loop are observed for the higher T_{sub} samples. The output curves for the homologue devices recorded in the saturation regime (i.e., using a drain-source voltage, V_{DS} , fixed to 50 V) at different gate-source voltages, V_{GS} , (from -10 V to 50 V), are reported in Figure 10c,d. The ideal n-type behavior is evidenced by the presence of the crossover between the linear and saturation regime, predicted at $V_{GS} - V_{TH} = V_{DS}$,^[89] where V_{DS} is the drain-source voltage and V_{TH} is the threshold voltage, indicated by the dotted lines in the pictures. Similar behavior was observed under vacuum conditions (Figure SI.4, Supporting Information). All of the parameters of the devices, working either in air or under vacuum and either in the linear or saturation regimes, were determined as described in the Supporting Information and are reported in Table SI.3.

Technological processes commonly performed for device optimization, such as chemical purification of the commercial semiconductor material, postdeposition annealing, electrode and dielectric functionalization, were not carried out and are beyond the goal of this work. These are likely to be the reason for the relatively poor performance of the transistors.^[28,44,53,90] However, our main finding, obtained for the PDI8-CN2 films deposited on the SiO₂/Si substrate, can be generalized to films

on functionalized Si substrates. Indeed, the structural (by XRD) and morphological (by AFM) features of the PDI-8CN2 films on the bare SiO₂, and on hexamethyldisilazane (HMDS) and octadecyltrichlorosilano (OTS) treated SiO₂ substrates have been shown to be very similar, and the electron mobility of the PDI-8CN2 devices remains relatively constant for all of these substrates.^[53] The insensitivity of PDI-8CN2 to the chemical nature of the dielectric has to be ascribed to its high electron affinity, which prevents an efficient electron trapping by the silanol groups present at the SiO₂ dielectric interface, quenching the n-channel FET activity.^[28,91]

The T_{sub} dependence of the device performance was evidenced by the analysis of the charge-carrier mobility, μ , and of the I_{ON}/I_{OFF} ratio calculated from the transfer curves. Regardless of the measurement conditions (i.e., in air or under vacuum, and both in the linear and the saturation regimes) and film thickness, by increasing T_{sub} , both μ and I_{ON}/I_{OFF} ratios increased by one order of magnitude. For instance, in the case of the measurements performed in air, in the linear regime ($V_{DS} = 5$ V), μ increased from $\approx 2 \times 10^{-3}$ cm² V⁻¹ s⁻¹ to $\approx 1 \times 10^{-2}$ cm² V⁻¹ s⁻¹

and I_{ON}/I_{OFF} ratio changed from $\approx 2 \times 10^4$ to $\approx 1 \times 10^5$, with the values having been averaged over the three film t .

The observed dependence of μ and of I_{ON}/I_{OFF} ratio on T_{sub} can be ascribed to the crystalline structure, morphology and growth mode of the PDI8-CN2 films. Indeed, the higher T_{sub} was shown to induce: i) a higher crystalline order, lower mosaicity and larger lateral domains (as found from XRD measurements); and ii) a lower grain-boundary density, a larger correlation length and a 2D growth mode (as determined by analysis of the AFM images). All of these features contribute to the improvement of the device performance, μ and I_{ON} , but they do not alter the OFF currents (the OFF current was calculated in device depletion mode and attained values of 10^{-10} A in air and 10^{-9} – 10^{-8} A under vacuum, as limited by the electrometer resolution). The intimate relationship between high structural order and efficient transport has been widely reported,^[92–94] and, in particular, the FWHM of the RCs is taken as a key parameter of the degree of structural order,^[95,96] having a very strong influence on mobility: in fact, the width mobility varies over orders of magnitude for small variations of the rocking width. In our system, the dependence of μ on the FWHM is clearly shown when comparing the data recorded at $T_{sub} = RT$ and 120 °C in all of the measurements conditions (Figure SI.5, Supporting Information).

Interestingly, μ values measured in air, μ_{air} , maintained the same order of magnitude as those in vacuum μ_{vac} , never decreasing by more than half the value of the μ_{vac} . This is a strong indication of the ambient stability of the PDI8-CN2 FETs reported in the literature.^[35]

To conclude, in this paper we have established, by means of non-conventional powder diffraction methods, the arrangement

of PDI8-CN2 molecules in the bulk material. We have verified that the same crystal phase forms in thin films sublimated on SiO₂/Si wafer, the pronounced thermodynamic stability of the bulk phase preventing the formation of a thin-film phase and the occurrence of polymorphism, detrimental to the transistor performances.^[37] The PDI8-CN2 molecules orient with the π -stacking direction parallel to the surface, resulting in good mobility characteristics for OTFTs in parallel configuration. Knowledge of the molecular organization was the starting point to exploring the relationship between the structural and morphological features of the thin films and their performance in devices. With this aim, we tuned the film structure and morphology by changing the substrate temperature (RT, 80 °C and 120 °C) and film thickness. By combining XRD and AFM analyses, we identified the two T_{sub} regimes, at low temperature (RT) and high temperature (80 °C and 120 °C), characterized by quite different features. The analysis of the AFM images allowed us to extract the parameters essential for identifying the molecular growth mechanism, namely the exponents (β and α) of the power laws predicted by DST: at high T_{sub} a layer-by-layer mechanism dominates, whereas a 3D-growth mode occurs at RT. The different growth mechanisms result in the morphological and structural features of the films and appear to be correlated with the trend of the electrical parameters measured in PDI8-CN2-based OTFTs.

5. Experimental Section

Thin-Film Deposition: PDI8-CN2 films of three different thicknesses (10 nm, 40 nm and 100 nm) were deposited by HVS (base pressure $P = 8 \times 10^{-8}$ mbar) at a rate of $12.5 \text{ \AA min}^{-1}$ on a 200 nm-thick SiO₂ substrate, thermally grown on a (001) Si wafer. Three series of films were prepared by keeping the substrates, respectively, at RT, 80 °C and 120 °C during the deposition. Simultaneously, in the same high-vacuum (HV) chamber, PDI8-CN2 films were deposited on test patterns to obtain bottom-contact bottom-gate OTFTs. The PDI8-CN2 source powder was used as provided by BASF without any further purification processes. Both the test patterns and the bare SiO₂ substrates were previously cleaned using a 15 min piranha etching (1:1 H₂O₂:H₂SO₄ solution kept at 150 °C) followed by a fast-lasting bath in 4% HF solution, rinsing in deionized water and drying in a nitrogen stream.

X-Ray Powder Diffraction: The non-conventional and complete crystal structure determination process from laboratory powder diffraction data is described in detail in the Supporting Information. Two sets of diffraction experimental set-ups were used, aimed at obtaining independent, complementary information that a single data collection could not provide: a Debye–Scherrer diffractometer (pattern 1), equipped with a glass capillary holder, and a conventional parafocusing Bragg–Brentano θ : θ goniometer (pattern 2), with flat-sample geometry. Crystal data for PDI8-CN2: C₄₂H₄₀N₄O₄, f.w. = 664.81 g mol⁻¹, 298 K, $\lambda = 1.540596 \text{ \AA}$, triclinic, space group P-1, $a = 5.0194(4) \text{ \AA}$, $b = 8.8409(7) \text{ \AA}$, $c = 20.195(1) \text{ \AA}$, $\alpha = 101.507(5)^\circ$, $\beta = 92.328(5)^\circ$, $\gamma = 100.154(5)^\circ$, $V = 861.7(1) \text{ \AA}^3$, $Z = 1$, $\rho_{\text{calc}} = 1.281 \text{ g cm}^{-3}$, $\mu (\text{Cu K}) = 0.66 \text{ mm}^{-1}$, $R_p = 0.073$, $R_{\text{wp}} = 0.107$; $R_{\text{Bragg}} = 0.052$ and 0.036 and 2θ ranges from 6 to 60° and from 6 to 80°, for patterns 1 and 2, respectively. Crystallographic data (excluding structure factors) for the structure(s) reported in this paper have been deposited with the Cambridge Crystallographic Data Centre as supplementary publication no. CCDC-833431.

X-Ray Diffraction on Thin Films: The thin films were characterized by X-ray reflectivity (XRR) and XRD measurements, both in out-of-plane and GID geometries, performed using a SmartLab-Rigaku diffractometer equipped with a rotating anode (Cu K α , $\lambda = 1.54180 \text{ \AA}$), followed by a

parabolic mirror to collimate the incident beam, and a series of variable slits (placed before and after the sample position). The 2D-GID images were recorded at the XRD1 beamline at the Elettra synchrotron facility at Trieste (Italy) using a monochromatic beam with a wavelength of 0.8499 \AA . The incident angle of the X-ray beam, α_i , was chosen below or above the critical angle for total reflection of the organic film (i.e., 0.12°). In this way, the contribution to the diffraction pattern coming from the upper layers of the organic film could be discriminated from that coming from the whole organic film. The diffraction patterns were recorded using a 2D camera (Pilatus detector) placed normal to the incident beam direction.

Atomic Force Microscopy: The morphology of the thin films deposited on the test pattern substrates was studied by collecting AFM images in air in semicontact mode using an NT-MDT Smena microscope equipped with Nanosensors GmbH NSG10 cantilevers. The statistical analysis was performed on four AFM images recorded for each film using Gwyddion software.^[97]

Electrical Measurements: The test patterns, fabricated by Fondazione Bruno Kessler, Trento, were composed of a heavily n-doped Si wafer (Gate) covered with a 200 nm-thick thermally grown layer of SiO₂, which acted as a gate dielectric, and with interdigitated, gold source-drain contacts. Each substrate contained two pairs of active channels characterized by the ratio $W/L = 550$, where W is the channel width, and L the channel length. In order to obtain the same high W/L ratio, two values of W (11 200 μm and 22 400 μm) and L (20 μm and 40 μm) were chosen. The OTFT characteristics were measured using a Keithley 2612A dual-channel Source Meter.

Ab Initio Calculations: Starting from the molecular geometry extracted from the experimental crystal structures of a series of PDI- n benchmark compounds^[46,51,52] and of PDI8-CN2 (this work), the minimum-energy geometry was determined using the GAUSSIAN03 program,^[98] with the B3LYP/6-31G* combination of density functional and basis set.

Molecular Mechanics Calculations: Lattice energy minimizations were performed using the GULP program^[99] for fully flexible molecules. The intramolecular interactions were described by harmonic potentials for bond stretching and bending, or by trigonometric potential functions for torsions.^[100] The intermolecular interactions were represented by an atom-atom potential with Lennard-Jones and electrostatic terms with electrostatic potential (ESP)^[98] atomic charges fitted to the ab initio B3LYP/6-31G* electrostatic potential. The parameters of the intra- and intermolecular potentials were taken from the DREIDING force field.^[100]

Search Procedure: In our standard procedure for predicting crystal structures,^[55,56,101] we systematically searched the potential energy hypersurface to identify its local minima, which represent the “natural” structures the crystalline system can exhibit.^[102] For PDI8-CN2, 5000 crystal configurations were generated, with known lattice and molecular parameters (Supporting Information), but different quasi-random orientations.^[103] The total lattice energy for each configuration was minimized and all of the distinct minima, with lattice parameters constrained to the experimental values, were identified. Finally, the energy minimization continued unconstrained, by also adjusting the unit cell axes and angles. The idea was, that, with a realistic potential model, the experimental structures should be close to the local minima of the potential energy.

Supporting Information

Supporting Information is available from the Wiley Online Library or from the author.

Acknowledgements

The authors acknowledge Dr. Silke Koehler (BASF Schweiz AG) for material supply and fruitful discussion and Dr. Luisa Barba and Dr. Gianmichele Arrighetti for their excellent support during the experiments

performed at Elettra. This work was supported by the EU Large Project One-P (FP7-NMP-2007-212311).

Received: July 16, 2011

Revised: October 9, 2011

Published online: December 20, 2011

- [1] C. D. Dimitrakopoulos, P. R. L. Malenfant, *Adv. Mater.* **2002**, *14*, 99.
- [2] S. R. Forrest, *Nature* **2004**, *428*, 911.
- [3] M. Halik, H. Klauk, U. Zschieschang, G. Schmid, C. Dehm, M. Schutz, S. Maisch, F. Effenberger, M. Brunnbauer, F. Stellacci, *Nature* **2004**, *431*, 963.
- [4] C. Kim, A. Facchetti, T. J. Marks, *Science* **2007**, *318*, 76.
- [5] Y. Y. Noh, N. Zhao, M. Caironi, H. Sirringhaus, *Nat. Nanotechnol.* **2007**, *2*, 784.
- [6] M. F. Calhoun, J. Sanchez, D. Olaya, M. E. Gershenson, V. Podzorov, *Nat. Mater.* **2008**, *7*, 84.
- [7] J. H. Cho, J. Lee, Y. Xia, B. Kim, Y. Y. He, M. J. Renn, T. P. Lodge, C. D. Frisbie, *Nat. Mater.* **2008**, *7*, 900.
- [8] D. J. Gundlach, J. E. Royer, S. K. Park, S. Subramanian, O. D. Jurchescu, B. H. Hamadani, A. J. Moad, R. J. Kline, L. C. Teague, O. Kirillov, C. A. Richter, J. G. Kushmerick, L. J. Richter, S. R. Parkin, T. N. Jackson, J. E. Anthony, *Nat. Mater.* **2008**, *7*, 216.
- [9] M. Novak, A. Ebel, T. Meyer-Friedrichsen, A. Jedaa, B. F. Vieweg, G. A. Yang, K. Voitchovsky, F. Stellacci, E. Spiecker, A. Hitsch, M. Halik, *Nano Lett.* **2011**, *11*, 156.
- [10] J. A. Rogers, Z. Bao, K. Baldwin, A. Dodabalapur, B. Crone, V. R. Raju, V. Kuck, H. Katz, K. Amundson, J. Ewing, P. Drzaic, *Proc. Natl. Acad. Sci. USA* **2001**, *98*, 4835.
- [11] G. H. Gelinck, H. E. A. Huitema, E. Van Veenendaal, E. Cantatore, L. Schrijnemakers, J. B. P. H. Van der Putten, T. C. T. Geuns, M. Beenhakkers, J. B. Giesbers, B. H. Huisman, E. J. Meijer, E. M. Benito, F. J. Touwslager, A. W. Marsman, B. J. E. Van Rens, D. M. De Leeuw, *Nat. Mater.* **2004**, *3*, 106.
- [12] M. A. McCarthy, B. Liu, E. P. Donoghue, I. Kravchenko, D. Y. Kim, F. So, A. G. Rinzier, *Science* **2011**, *332*, 570.
- [13] A. R. Brown, A. Pomp, C. M. Hart, D. M. Deleeuw, *Science* **1995**, *270*, 972.
- [14] B. Crone, A. Dodabalapur, A. Gelperin, L. Torsi, H. E. Katz, A. J. Lovinger, Z. Bao, *Appl. Phys. Lett.* **2001**, *78*, 2229.
- [15] J. Janata, M. Josowicz, *Nat. Mater.* **2003**, *2*, 19.
- [16] X. F. Guo, M. Myers, S. X. Xiao, M. Lefenfeld, R. Steiner, G. S. Tulevski, J. Y. Tang, J. Baumert, F. Leibfarth, J. T. Yardley, M. L. Steigerwald, P. Kim, C. Nuckolls, *Proc. Natl. Acad. Sci. USA* **2006**, *103*, 11452.
- [17] M. E. Roberts, S. C. B. Mannsfeld, N. Queralto, C. Reese, J. Locklin, W. Knoll, Z. N. Bao, *Proc. Natl. Acad. Sci. USA* **2008**, *105*, 12134.
- [18] B. Crone, A. Dodabalapur, Y. Y. Lin, R. W. Filas, Z. Bao, A. LaDuca, R. Sarpeshkar, H. E. Katz, W. Li, *Nature* **2000**, *403*, 521.
- [19] T. D. Anthopoulos, S. Setayesh, E. Smits, M. Colle, E. Cantatore, B. de Boer, P. W. M. Blom, D. M. de Leeuw, *Adv. Mater.* **2006**, *18*, 1900.
- [20] H. Klauk, U. Zschieschang, J. Pflaum, M. Halik, *Nature* **2007**, *445*, 745.
- [21] A. Facchetti, *Nat. Mater.* **2008**, *7*, 839.
- [22] M. M. Payne, S. R. Parkin, J. E. Anthony, C. C. Kuo, T. N. Jackson, *J. Am. Chem. Soc.* **2005**, *127*, 4986.
- [23] H. Ebata, T. Izawa, E. Miyazaki, K. Takimiya, M. Ikeda, H. Kuwabara, T. Yui, *J. Am. Chem. Soc.* **2007**, *129*, 15732.
- [24] P. Gao, D. Beckmann, H. N. Tsao, X. L. Feng, V. Enkelmann, M. Baumgarten, W. Pisula, K. Mullen, *Adv. Mater.* **2009**, *21*, 213.
- [25] A. S. Dhoot, J. D. Yuen, M. Heeney, I. McCulloch, D. Moses, A. J. Heeger, *Proc. Natl. Acad. Sci. USA* **2006**, *103*, 11834.
- [26] H. L. Pan, Y. N. Li, Y. L. Wu, P. Liu, B. S. Ong, S. P. Zhu, G. Xu, *J. Am. Chem. Soc.* **2007**, *129*, 4112.
- [27] I. McCulloch, M. Heeney, C. Bailey, K. Genevicius, I. Macdonald, M. Shkunov, D. Sparrowe, S. Tierney, R. Wagner, W. M. Zhang, M. L. Chabynyc, R. J. Kline, M. D. McGehee, M. F. Toney, *Nat. Mater.* **2006**, *5*, 328.
- [28] B. A. Jones, A. Facchetti, M. R. Wasielewski, T. J. Marks, *J. Am. Chem. Soc.* **2007**, *129*, 15259.
- [29] Y. G. Wen, Y. Q. Liu, *Adv. Mater.* **2010**, *22*, 1331.
- [30] H. E. Katz, A. J. Lovinger, J. Johnson, C. Kloc, T. Siegrist, W. Li, Y. Y. Lin, A. Dodabalapur, *Nature* **2000**, *404*, 478.
- [31] H. Yan, Z. H. Chen, Y. Zheng, C. Newman, J. R. Quinn, F. Dotz, M. Kastler, A. Facchetti, *Nature* **2009**, *457*, 679.
- [32] H. Usta, C. Risko, Z. M. Wang, H. Huang, M. K. Delimeroglu, A. Zhukhovitskiy, A. Facchetti, T. J. Marks, *J. Am. Chem. Soc.* **2009**, *131*, 5586.
- [33] B. Yoo, B. A. Jones, D. Basu, D. Fine, T. Jung, S. Mohapatra, A. Facchetti, K. Dimmler, M. R. Wasielewski, T. J. Marks, A. Dodabalapur, *Adv. Mater.* **2007**, *19*, 4028.
- [34] Z. J. Chen, M. G. Debije, T. Debaerdemaeker, P. Osswald, F. Wurthner, *ChemPhysChem* **2004**, *5*, 137.
- [35] B. A. Jones, M. J. Ahrens, M. H. Yoon, A. Facchetti, T. J. Marks, M. R. Wasielewski, *Angew. Chem. Int. Ed.* **2004**, *43*, 6363.
- [36] R. J. Chesterfield, J. C. McKeen, C. R. Newman, P. C. Ewbank, D. A. da Silva, J. L. Bredas, L. L. Miller, K. R. Mann, C. D. Frisbie, *J. Phys. Chem. B* **2004**, *108*, 19281.
- [37] R. J. Chesterfield, J. C. McKeen, C. R. Newman, C. D. Frisbie, P. C. Ewbank, K. R. Mann, L. L. Miller, *J. Appl. Phys.* **2004**, *95*, 6396.
- [38] D. J. Gundlach, K. P. Pernstich, G. Wilckens, M. Gruter, S. Haas, B. Batlogg, *J. Appl. Phys.* **2005**, *98*, 064502.
- [39] R. Schmidt, J. H. Oh, Y. S. Sun, M. Deppisch, A. M. Krause, K. Radacki, H. Braunschweig, M. Konemann, P. Erk, Z. A. Bao, F. Wurthner, *J. Am. Chem. Soc.* **2009**, *131*, 6215.
- [40] C. Piliego, F. Cordella, D. Jarzab, S. Lu, Z. Chen, A. Facchetti, M. A. Loi, *Appl. Phys. A - Mater. Sci. Process.* **2009**, *95*, 303.
- [41] A. S. Molinari, H. Alves, Z. Chen, A. Facchetti, A. F. Morpurgo, *J. Am. Chem. Soc.* **2009**, *131*, 2462.
- [42] B. Yoo, T. Jung, D. Basu, A. Dodabalapur, B. A. Jones, A. Facchetti, M. R. Wasielewski, T. J. Marks, *Appl. Phys. Lett.* **2006**, *88*, 082104.
- [43] B. Yoo, A. Madgavkar, B. A. Jones, S. Nadkarni, A. Facchetti, K. Dimmler, M. R. Wasielewski, T. J. Marks, A. Dodabalapur, *IEEE Electron. Device Lett.* **2006**, *27*, 737.
- [44] J. Rivnay, L. H. Jimison, J. E. Northrup, M. F. Toney, R. Noriega, S. F. Lu, T. J. Marks, A. Facchetti, A. Salleo, *Nat. Mater.* **2009**, *8*, 952.
- [45] H. Yan, Y. Zheng, R. Blache, C. Newman, S. Lu, J. Woerle, A. Facchetti, *Adv. Funct. Mat.* **2008**, *20*, 3393.
- [46] Parafocusing Bragg-Brentano grants high-resolution and quite narrow peaks but high preferred-orientation effects, whereas Debye-Scherrer geometry, mounting a glass capillary loaded with ground PD18-CN2 crystals, affords correct estimates of the measured intensities, at the expense of evident peak broadening (by sample-effect contribution).
- [47] E. Hadicke, F. Graser, *Acta Crystallogr. C* **1986**, *42*, 195.
- [48] H. Lipson, A. R. Stokes, *Proc. R. Soc. London. A* **1942**, *181*, 101.
- [49] Apparently, as derived from the preferred orientation coefficients employed in matching the experimental versus the calculated data for the X-ray trace collected in flat-plate geometry, the needles elongate approximately in the [100] direction, a not-so-obvious, and difficult-to-interpret, direction. However, a few tests performed with different preferred orientation poles within the March-Dollase formulation show that the alternative [−651] choice is only partially detrimental to the overall fitting, thus suggesting the possible coincidence of the stacking and needle growth directions.

- [50] A. Z. March, *Kristallografiya* **1932**, *81*, 285.
- [51] W. A. Dollase, *J. Appl. Crystallogr.* **1987**, *19*, 267.
- [52] M. Kasha, H. R. Rawls, M. A. El-Bayoumi, *Pure Appl. Chem.* **1965**, *11*, 371.
- [53] B. A. Jones, A. Facchetti, M. R. Wasielewski, T. J. Marks, *Adv. Funct. Mater.* **2008**, *18*, 1329.
- [54] A. L. Briseno, S. C. B. Mannsfeld, C. Reese, J. M. Hancock, Y. Xiong, S. A. Jenekhe, Z. Bao, Y. Xia, *Nano Lett.* **2007**, *7*, 2847.
- [55] R. G. Della Valle, E. Venuti, A. Brillante, A. Girlando, *J. Phys. Chem. A* **2006**, *110*, 10858.
- [56] R. G. Della Valle, E. Venuti, A. Brillante, A. Girlando, *J. Phys. Chem. A* **2008**, *112*, 6715.
- [57] B. E. Warren, *X-Ray Diffraction*, Dover, New York **1990**.
- [58] B. Nickel, R. Barabash, R. Ruiz, N. Koch, A. Kahn, L. C. Feldman, R. F. Haglund, G. Scoles, *Phys. Rev. B: Condens. Matter* **2004**, *70*, 125401.
- [59] J. A. Merlo, C. R. Newman, C. P. Gerlach, T. W. Kelley, D. V. Muires, S. E. Fritz, M. F. Toney, C. D. Frisbie, *J. Am. Chem. Soc.* **2005**, *127*, 3997.
- [60] D. W. Breiby, O. Bunk, J. W. Andreasen, H. T. Lemke, M. M. Nielsen, *J. Appl. Crystallogr.* **2008**, *41*, 262.
- [61] T. N. Krauss, E. Barrena, D. G. de Oteyza, X. N. Zhang, J. Major, V. Dehm, F. Wurthner, H. Dosch, *J. Phys. Chem. C* **2009**, *113*, 4502.
- [62] T. N. Krauss, E. Barrena, X. N. Zhang, D. G. de Oteyza, J. Major, V. Dehm, F. Wurthner, L. P. Cavalcanti, H. Dosch, *Langmuir* **2008**, *24*, 12742.
- [63] R. A. Cormier, B. A. Gregg, *J. Phys. Chem. B* **1997**, *101*, 11004.
- [64] C. W. Struijk, A. B. Sieval, J. E. J. Dakhorst, M. van Dijk, P. Kimkes, R. B. M. Koehorst, H. Donker, T. J. Schaafsma, S. J. Picken, A. M. van de Craats, J. M. Warman, H. Zuilhof, E. J. R. Sudholter, *J. Am. Chem. Soc.* **2000**, *122*, 11057.
- [65] J. Krug, *Physica A* **2004**, *340*, 647.
- [66] A. C. Durr, F. Schreiber, K. A. Ritley, V. Kruppa, J. Krug, H. Dosch, B. Struth, *Phys. Rev. Lett.* **2003**, *90*, 647.
- [67] S. Kowarik, A. Gerlach, A. Hinderhofer, S. Milita, F. Borgatti, F. Zontone, T. Suzuki, F. Biscarini, F. Schreiber, *Phys. Status Solidi Rapid Res. Lett.* **2008**, *2*, 120.
- [68] G. X. Zhang, B. L. Weeks, M. Holtz, *Surf. Sci.* **2011**, *605*, 463.
- [69] J. P. Schlomka, M. Tolan, W. Press, *Appl. Phys. Lett.* **2000**, *76*, 2005.
- [70] J. Krug, M. Plischke, M. Siegert, *Phys. Rev. Lett.* **1993**, *70*, v3271.
- [71] Z. W. Lai, S. Dassarma, *Phys. Rev. Lett.* **1991**, *66*, 2348.
- [72] J. M. Kim, S. Dassarma, *Phys. Rev. E* **1995**, *51*, 1889.
- [73] A. E. Lita, J. E. Sanchez, *Phys. Rev. B: Condens. Matter* **2000**, *61*, 7692.
- [74] S. Dassarma, S. V. Ghaisas, *Phys. Rev. Lett.* **1992**, *69*, 3762.
- [75] F. Biscarini, P. Samori, O. Greco, R. Zamboni, *Phys. Rev. Lett.* **1997**, *78*, 2389.
- [76] G. Rasigni, M. Rasigni, J. Palmari, C. Dussert, F. Varnier, A. Llebaria, *J. Opt. Soc. Am. A* **1988**, *5*, 99.
- [77] F. Biscarini, R. Zamboni, P. Samori, P. Ostojia, C. Taliani, *Phys. Rev. B: Condens. Matter* **1995**, *52*, 14868.
- [78] F. Biscarini, O. Greco, A. Lauria, R. Zamboni, C. Taliani, *Mol. Cryst. Liq. Cryst. A* **1996**, *290*, 203.
- [79] M. Beigmohamadi, P. Niyamakom, A. Farahzadi, C. Effertz, S. Kremers, D. Brueggemann, M. Wuttig, *J. Appl. Phys.* **2008**, *104*, 013505.
- [80] P. H. Dederichs, *Phys. Rev. B: Condens. Matter* **1971**, *4*, 1041.
- [81] P. Ehrhart, H. Trinkaus, *Phys. Rev. B: Condens. Matter* **1982**, *52*, 834.
- [82] M. Beigmohamadi, P. Niyamakom, A. Farahzadi, S. Kremers, T. Michely, M. Wuttig, *Phys. Status Solidi Rapid Res. Lett.* **2008**, *2*, 1.
- [83] R. Ruiz, A. C. Mayer, G. G. Malliaras, B. Nickel, G. Scoles, A. Kazimirov, H. Kim, R. L. Headrick, Z. Islam, *Appl. Phys. Lett.* **2004**, *85*, 4926.
- [84] A. Brillante, I. Bilotti, R. G. Della Valle, E. Venuti, A. Girlando, *CrystEngComm* **2008**, *10*, 937.
- [85] A. Brillante, I. Bilotti, R. G. Della Valle, E. Venuti, S. Milita, C. Dionigi, F. Borgatti, A. N. Lazar, F. Biscarini, M. Mas-Torrent, N. S. Oxtoby, N. Crivillers, J. Veciana, C. Rovira, M. Leufgen, G. Schmidt, L. W. Molenkamp, *CrystEngComm* **2008**, *10*, 1899.
- [86] R. Pfattner, M. Mas-Torrent, I. Bilotti, A. Brillante, S. Milita, F. Liscio, F. Biscarini, T. Marszalek, J. Ullanski, A. Nosal, M. Gazicki-Lipman, M. Leufgen, G. Schmidt, L. W. Molenkamp, V. Laukhin, J. Veciana, C. Rovira, *Adv. Mater.* **2010**, *22*, 4198.
- [87] S. Milita, M. Servidori, F. Ciccoira, C. Santato, A. Pifferi, *Nucl. Instrum. Methods B* **2006**, *246*, 101.
- [88] J. F. Moulin, F. Dinelli, M. Massi, C. Albonetti, R. Kshirsagar, F. Biscarini, *Nucl. Instrum. Methods Phys. Res. B* **2006**, *246*, 122.
- [89] Z. Bao, J. Locklin, *Organic Field-Effect Transistors*, CRC Press, Boca Raton, FL **2007**.
- [90] K. J. Baeg, D. Khim, J. H. Kim, M. Kang, I. K. You, D. Y. Kim, Y. Y. Noh, *Org. Electron.* **2011**, *12*, 634.
- [91] L. L. Chua, J. Zaumseil, J. F. Chang, E. C. W. Ou, P. K.-H. Ho, H. Sirringhaus, R. H. Friend, *Nature* **2005**, *434*, 194.
- [92] G. Horowitz, *Adv. Mater.* **1998**, *10*, 365.
- [93] M. C. J. M. Vissenberg, M. Matters, *Phys. Rev. B: Condens. Matter* **1998**, *57*, 12964.
- [94] A. C. Durr, F. Schreiber, M. Munch, N. Karl, B. Krause, V. Kruppa, H. Dosch, *Appl. Phys. Lett.* **2002**, *81*, 2276.
- [95] N. Karl, *Synth. Met.* **2003**, *133*, 649.
- [96] A. R. Brown, D. M. Deleeuw, E. J. Lous, E. E. Havinga, *Synth. Met.* **1994**, *66*, 257.
- [97] Gwyddion Scan Probe Microscopy data analysis software.
- [98] M. J. Frisch, G. W. Trucks, H. B. Schlegel, G. E. Scuseria, M. A. Robb, J. R. Cheeseman, J. A. Montgomery Jr., T. Vreven, K. N. Kudin, J. C. Burant, J. M. Millam, S. S. Iyengar, J. Tomasi, V. Barone, B. Mennucci, M. Cossi, G. Scalmani, N. Rega, G. A. Petersson, H. Nakatsuji, M. Hada, M. Ehara, K. Toyota, R. Fukuda, J. Hasegawa, M. Ishida, T. Nakajima, Y. Honda, O. Kitao, H. Nakai, M. Klene, X. Li, J. E. Knox, H. P. Hratchian, J. B. Cross, V. Bakken, C. Adamo, J. Jaramillo, R. Gomperts, R. E. Stratmann, O. Yazyev, A. J. Austin, R. Cammi, C. Pomelli, J. W. Ochterski, P. Y. Ayala, K. Morokuma, G. A. Voth, P. Salvador, J. J. Dannenberg, V. G. Zakrzewski, S. Dapprich, A. D. Daniels, M. C. Strain, O. Farkas, D. K. Malick, A. D. Rabuck, K. Raghavachari, J. B. Foresman, J. V. Ortiz, Q. Cui, A. G. Baboul, S. Clifford, J. Cioslowski, B. B. Stefanov, G. Liu, A. Liashenko, P. Piskorz, I. Komaromi, R. L. Martin, D. J. Fox, T. Keith, M. A. Al-Laham, C. Y. Peng, A. Nanayakkara, M. Challacombe, P. M. W. Gill, B. Johnson, W. Chen, M. W. Wong, C. Gonzalez, J. A. Pople, *Gaussian 03, Revision D.02*, Gaussian, Inc., Wallingford, CT **2004**.
- [99] J. D. Gale, A. L. Rohl, *Mol. Simul.* **2003**, *29*, 291.
- [100] S. L. Mayo, B. D. Olafson, W. A. Goddard, *J. Phys. Chem.* **1990**, *94*, 8897.
- [101] R. G. Della Valle, E. Venuti, A. Brillante, A. Girlando, *J. Chem. Phys.* **2003**, *118*, 807.
- [102] F. H. Stillinger, T. A. Weber, *Phys. Rev. A: At. Mol. Optical Phys.* **1982**, *25*, 978.
- [103] W. H. Press, S. A. Teukolsky, W. T. Vetterling, B. P. Flannery, *Numerical Recipes in Fortran*, Cambridge University Press, Cambridge, UK **1992**.